

# Analysis of Gamma Titanium Aluminide Welds Produced by Gas Tungsten Arc Welding

*Careful selection of GTAW parameters is needed for successful joining of TiAl alloys*

BY M. F. ARENAS AND V. L. ACOFF

**ABSTRACT.** This study examines the weldability of a cast gamma titanium aluminide ( $\gamma$ -TiAl) alloy using the autogenous gas tungsten arc welding process. Experimentation consisted of spot and butt-joint welding of gamma titanium aluminides at welding current levels ranging from 50 to 150 A using no preheating. It was found that the welded microstructure exhibited columnar and equiaxed dendritic structures along with a small quantity of gamma grains. A closer examination of the dendritic grains showed that a fine lamellar structure consisting of alternating platelets of alpha-2 and gamma was observed within the dendrites. Other microstructural constituents in the fusion zone were a massive gamma structure and the alpha-2 phase. Crack-free welds were obtained for high welding currents. However, cracking was observed at lower welding currents, which also corresponded to increased amounts of the alpha-2 phase. The hardness of the fusion zone was increased relative to the base metal, resulting in reduction in both room temperature ductility and tensile strength of the weld. Conclusively, very careful selection of welding parameters that result in decreased amounts of the alpha-2 phase is required for successful joining of TiAl alloys using gas tungsten arc welding.

## Introduction

The low density, superior strength, and high stiffness at elevated temperatures of TiAl intermetallic alloys have attracted a great deal of attention from the aerospace and automobile industries (Refs. 1-5). However, it is apparent that the ability to weld these materials to themselves and to other materials is the key to making them

*M. F. ARENAS is a Postdoctoral Fellow and V. L. ACOFF is an Associate Professor in the Department of Metallurgical and Materials Engineering, University of Alabama, Tuscaloosa, Ala.*

more attractive. It is particularly interesting to study the feasibility of using the gas tungsten arc welding (GTAW) technique, which promises to be an economical way to weld gamma titanium aluminides. Despite its importance, only a few papers have been published on the joining of gamma titanium aluminides using gas tungsten arc welding. For instance, L. C. Mallory et al. (Refs. 6, 7) investigated the evolution of the weld fusion zone and heat-affected zone (HAZ) microstructure in preheated GTA welds of a forged gamma Ti-48Al-2Cr-2Nb alloy. When preheating to 800°C was used, no cracking was detected. However, weld beads produced under identical welding conditions but without preheating all contained cracks. A microstructural analysis of the fusion zone showed cored dendritic solidification structures with single colonies of fine lamellar alpha-2/gamma ( $\alpha_2/\gamma$ ) constituent extending across the dendrites. The occasional presence of interdendritic gamma grains was also observed. Interestingly, the microhardness of the fusion zone and HAZ were significantly increased relative to the base metal.

T. J. Kelly (Ref. 8) studied the GTA weldability of a cast Ti-48Al-2Cr-2Nb gamma alloy. Prior to welding, all specimens underwent hot isostatic pressing (HIPing) and some were heat-treated after HIPing at 1300°C for 20 h. As-deposited weld metal exhibited a highly segregated solidification structure that consisted of the gamma phase, colonies of

gamma plus alpha-2 ( $\gamma + \alpha_2$ ) laminates, and the Laves phase. Solid-state cracking was observed in all welds of as-HIPed specimens even with preheats as high as 600°C. However, specimens heat-treated at 1300°C after HIPing did not crack even without preheating because heat-treating at 1300°C increased the ductility of the specimens. In another study, Bharani and Acoff (Ref. 9) used autogenous GTA spot welding to produce crack-free welds in cast alloy Ti-48Al-2Cr-2Nb and extruded alloy Ti-46Al-2Cr-2Nb-0.9Mo without the use of preheating. They showed it is possible to achieve crack-free welds by only applying a post-stress relief treatment at 615°C. The crack length in the fusion zone decreased as a function of increasing current level, with no cracks observed for the highest current levels. Dendritic solidification structures were produced in the fusion zone of both alloys. Microhardness profiles also indicated an increase in hardness from the base metal to the fusion zone.

Although some success has been achieved, a comprehensive understanding of the weldability of these alloys is still lacking. The objective of the present study is to analyze GTA welding of the intermetallic  $\gamma$ -TiAl by examining the structure and mechanical properties of  $\gamma$ -TiAl welds for different welding currents. Characterization tools and techniques employed for this investigation consisted of light microscopy, X-ray diffraction, scanning electron microscopy, transmission electron microscopy, microhardness testing, and tensile testing.

## Experimental Procedure

### Materials and Sample Preparation

An alloy of nominal composition Ti-48Al-2Nb-2Cr (at.-%) was used in this study, with the actual composition shown in Table 1. The alloy was received in the form of 256-mm-long  $\times$  110-mm wide  $\times$  15-

### KEY WORDS

Advanced Materials  
Ti Alloys  
GTAW  
Spot Welds  
Butt-Joint Welds

mm-thick cast plates from GE Aircraft Engines. The specimens were HIPed at 1185°C at 107 MPa for 3 h followed by a stabilization heat treatment at 1205°C for 2 h, which was all performed at GE. The cast plates were sectioned into 100-mm × 15-mm × 2-mm specimens for butt-joint welding and 20-mm × 15-mm × 2-mm specimens for spot welding (i.e., welding with the torch stationary at a single location for a fixed time) using electrical-discharge machining (EDM). The specimens were mechanically ground with 120-grit SiC paper then pickled in a solution composed of 400 mL H<sub>2</sub>O + 40 g KOH + 40 mL H<sub>2</sub>O<sub>2</sub> in order to remove surface contaminants. Before welding, a prestress relief treatment was performed at 615°C for 2 h to relieve any stress produced during grinding of the re-cast EDM layer.

### Experimental Apparatus

Autogenous GTA welds were produced using spot and butt-joint welding on coupons of  $\gamma$ -TiAl alloys. All welding experiments were performed using direct current electrode negative. A welding speed of 3 mm/s was used to make the butt-joint welds and a welding time of 2 s was employed for the spot welds. The welding equipment had a spot timer device that allowed precise control of the welding time. The welding currents used ranged from 50 to 150 A and the corresponding welding voltage was 14–18 V. Immediately after welding, the samples were visually checked to detect the presence of cracks. All welding was performed inside a welding chamber that was purged with argon for 10 min prior to welding.

### Materials Characterization

The welded and as-received samples were sectioned into metallographic specimens. These metallographic samples were prepared using conventional metallographic procedures for titanium aluminides (Ref. 10). Microstructural details were revealed by a Kroll's modified etching solution comprised of 100 mL H<sub>2</sub>O + 35 mL H<sub>2</sub>O<sub>2</sub> + 5 mL HNO<sub>3</sub> + 10 mL HF. Microstructural characterization was performed using light microscopy, scanning electron microscopy (SEM) equipped with energy dispersive X-ray spectrometry (EDS), and transmission electron microscopy (TEM). X-ray diffraction (XRD) was used for primary phase identification of the fusion zone and base metal. The welded specimens were prepared for XRD by carefully removing the fusion zone from the specimen using a precision saw. Measurement parameters for XRD were as follows: Cu K $\alpha$  radiation, accelerating voltage 40 kV, and tube

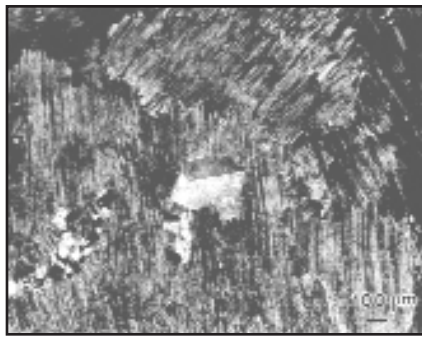


Fig. 1 — Light micrograph of the as-received microstructure.

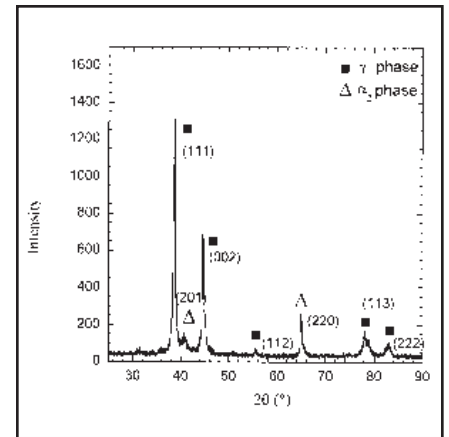


Fig. 2 — XRD pattern of the base metal.

Table 1 — Composition of the Titanium Alloy Used in This Study (Atomic Percent)

Ti	Al	Cr	Nb	Fe	Si	O	C
Bal.	48	1.8	1.8	0.02	0.004	0.22	0.04

current 35 mA. Diffraction patterns were obtained in the step, 2 $\theta$  mode in the range of 20–90 deg.

### Mechanical Testing

Microhardness data was obtained using a Knoop microhardness tester with a load of 500 g. The Knoop hardness number (KHN) was plotted as a function of distance across the welded specimen. Tensile tests were carried out on a universal testing machine at room temperature using a constant crosshead speed under a strain rate of 10<sup>-4</sup> s<sup>-1</sup>. Two tensile specimens were evaluated: one that consisted of only the base metal and the other of only the fusion zone.

## Results and Discussion

### Microstructural Characterization of the Base Metal

The as-received condition of the alloy consisted primarily of a lamellar microstructure composed of alternating platelets of gamma and alpha-2 and some equiaxed gamma grains, as shown in Fig. 1. This microstructure is the result of the treatment for cast alloys developed by Austin et al. (Ref. 11), which involves HIPing of the as-cast alloy followed by heat treatment in the alpha + gamma field. The X-ray diffraction analysis of the base metal is shown in Fig. 2. In this XRD scan, peaks due to gamma and alpha-2 phases are identified. The prominent peak at

about 39 deg corresponds to the gamma phase (Ref. 12) and it accounts for both the gamma lamellae and the equiaxed gamma grains observed. After solidification, cast gamma titanium aluminides are transformed into a lamellar structure with a preferred orientation of the lamellae — Fig. 1. The lamellae are aligned parallel to the outer surface of the ingot, i.e., perpendicular to the heat flow during solidification. This texture is reflected in the XRD measurement showing a high-intensity peak in the (111) plane. The small peak at about 41 deg corresponds to the alpha-2 phase (Ref. 13), which is present in the base metal as alpha-2 lamellae. The weak intensity of the alpha-2 peak is probably due to the very thin alpha-2 lamellae, which is below the spatial resolution of the XRD technique, and the minimal presence of individual alpha-2 grains as shown in Fig. 1.

### Fusion Zone Microstructures for Spot Welds

Figure 3 shows a light micrograph of a weld obtained by welding with an arc current of 50 A, where the evolution of microstructure from the base metal (left) to the fusion zone (right) is evident. This figure shows that the fusion zone microstructure was composed of columnar grains oriented perpendicular to the direction of the radial fusion boundary. This was expected, since during solidification, grains tend to grow in the direction perpendicular to the solid/liquid interface,

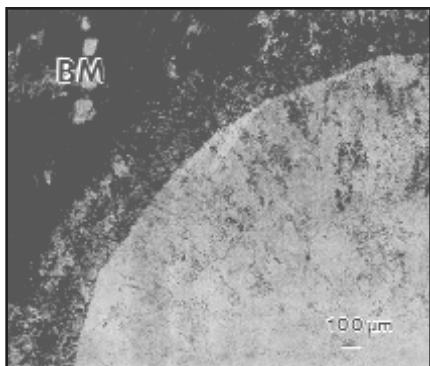


Fig. 3 — Light micrograph for the 50-A spot welded specimen. BM denotes base metal.

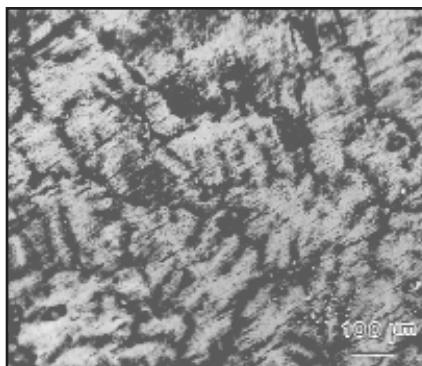


Fig. 4 — Higher magnification light micrograph of the columnar structure obtained for spot welding using a current of 50 A.

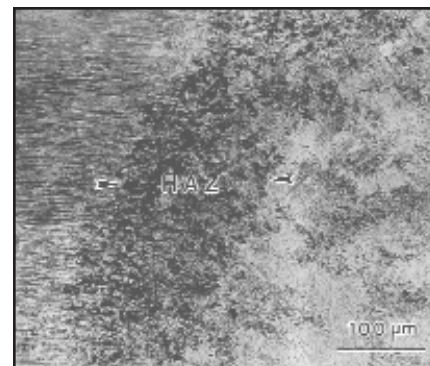


Fig. 5 — Light micrograph showing heat-affected zone for the 50-A spot welded specimen.

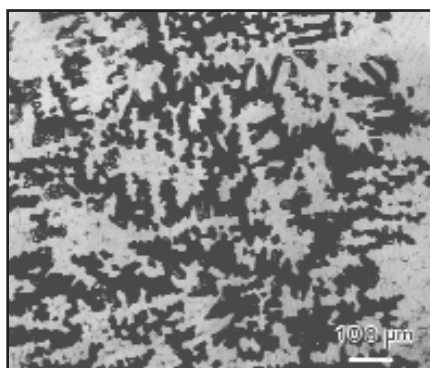


Fig. 6 — Light micrograph showing the center of the fusion zone for the 50-A specimen.

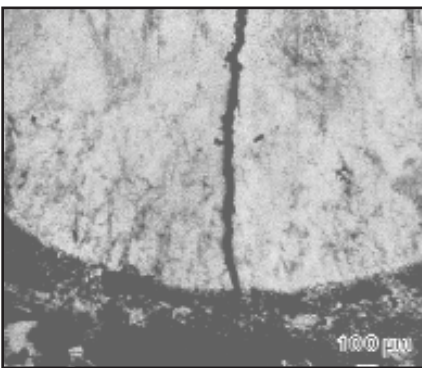


Fig. 7 — Light micrograph showing a solidification crack that developed for spot welding at 50 A.



Fig. 8 — Fusion zone microstructure for specimen butt-joint welded using a welding current of 55 A.

which is the direction of the maximum temperature gradient and thus the maximum driving force for solidification. Higher magnification micrographs of the columnar structure show lamellar grains and some amount of small blocky grains identified as the gamma phase — Fig. 4.

A region of about 200 μm between the base metal and the fusion zone can be recognized as the heat-affected zone (HAZ) — Fig. 5. This region mainly consisted of equiaxed gamma grains. The center of the fusion zone showed a markedly different microstructure. This region, which experienced the highest temperatures, exhibited a dendritic structure — Fig. 6. The difference in microstructure between the weld centerline and the fusion boundary can be attributed to different temperature gradients and solidification rates between the two regions. As the welding current was increased, the volume fraction of lamellar structure increased while that for the equiaxed gamma grains decreased.

A high cracking susceptibility was observed for welding at 50 A. A typical crack that occurred is shown in Fig. 7. The cracks appeared either immediately after

welding or several seconds after welding was performed. These cracks were identified as solidification cracks and occurred at the center of the fusion zone. For the spot welds, the center of the weld pool was highly susceptible to crack development and occasionally the cracks propagated into the base metal, as shown at the bottom of Fig. 7. Interestingly, SEM/EDS analysis found that the cracked surfaces were enriched with Al ranging from 51 to 54 at.-%, suggesting that the heavily segregated interdendritic regions were initiation sites for cracks.

Since the specimens were relatively small (2 mm thick) and there was little or no external stress exerted to the workpiece, it is believed the major contributing factor to the susceptibility to solidification cracking was thermal stresses. The thermal stresses developed from the difference in temperature across the fusion zone as a result of the metal at the fusion zone/base metal boundary solidifying much faster than the metal at the center of the fusion zone. The thermal stresses cannot be accommodated due to the lack of ductility of the fusion zone, which results

from the increased volume fraction of the brittle alpha-2 phase compared to the base metal. Furthermore, severe solute segregation at the center of the fusion zone provides fracture initiation sites for the cracks. However, it is believed that decreasing the cooling rate (increasing the welding current), which in turn reduces both alpha-2 formation and interdendritic segregation, reduces the susceptibility for solidification cracking. Traditional hot cracking was not the operative mechanism since no evidence of grain boundary liquation or fracture features associated with the occurrence of subsolid liquid microconstituents was observed.

No cracks were observed for using welding currents equal to or greater than 75 A. This observation supports the belief that decreasing the cooling rate by increasing the welding current reduces the susceptibility for solidification cracking. Although the butt-joint welded specimens have a much higher heat input compared to spot welded specimens, it was consistently observed that the specimens spot welded at 50 A exhibited solidification cracking, whereas specimens spot welded

at currents greater than or equal to 75 A did not. Patterson et al. (Ref. 14) concluded there is a critical weld cooling rate (300 K/s) below which cracking does not occur for  $\gamma$ -TiAl welds. They observed from light microscopy that an increase in the acicular microconstituent occurred with increasing the weld cooling rate. For the present study, a change in the fusion zone microstructure with increased welding current (decreased cooling rate) was also observed. As the welding current was increased, the volume fraction of the brittle  $\alpha$ -2 phase decreased. This microstructural observation was supported by the XRD results that are presented in the present study.

## Fusion Zone Microstructures for Butt-Joint Welds

Butt-joint welds were obtained using three different welding currents: 55, 75, and 115 A. Figure 8 shows the fusion zone microstructure obtained for the 55-A heat input. Large columnar grains oriented in the welding direction were observed. Similar features were also obtained for the other two heat inputs. However, an increase in the grain size of the columnar structure was evident as the welding current increased. Figure 9 shows a higher magnification SEM micrograph of the fusion zone microstructure produced for a welding current of 55 A. This microstructure mainly consisted of fine lamellar grains, similar to those observed for the spot welded specimens. Large gamma grains located at lamellar grain boundaries were also observed. Interestingly, some dark, deeply etched gamma grains with a patchy morphology were observed — Fig. 9B. These grains were identified as massive gamma grains ( $\gamma_m$ ), which result from the massive transformation from alpha to gamma at relatively high cooling rates (Ref. 15). Also, some amount of alpha-2 phase, resolvable only by TEM analysis, is believed to be present due to the higher cooling rate — Fig. 10. Figure 10A is a bright-field TEM micrograph of the fusion zone showing an alpha-2 grain with a neighboring lamellar grain. The identification of the phase was confirmed with a selected area diffraction pattern in the (0001) orientation as shown in Fig. 10B. The diffraction pattern confirmed the hexagonal close-packed alpha-2 structure. Interestingly, the heat-affected zone was practically indistinguishable at the optical and SEM scale for the butt-joint welded specimens. The 55-A specimen exhibited a high proportion of cracks. The crack morphology was similar to that observed for the 50-A spot welded specimen.

Increasing the welding current to 75 A revealed that the lamellar structure was

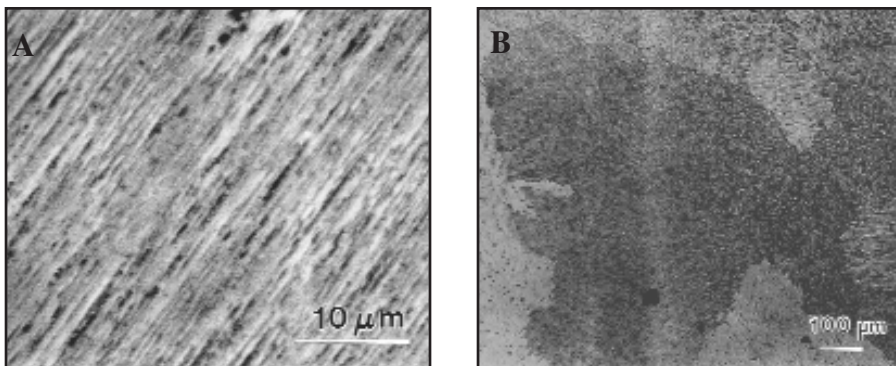


Fig. 9 — Fusion zone microstructures for the 55-A butt-joint welded specimen. A — SEM secondary electron image showing the fusion zone at a higher magnification; B — light micrograph showing a massive gamma grain.

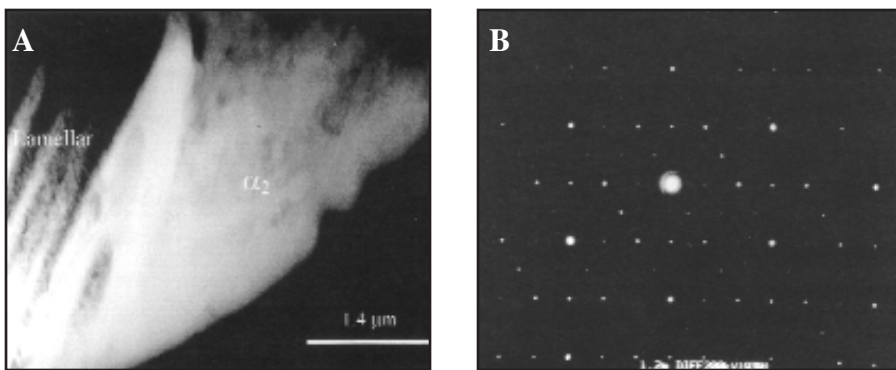


Fig. 10 — TEM micrograph of the fusion zone showing the alpha-2 phase. A — Bright-field image; B — selected area diffraction pattern of the region shown in A.

the main constituent. However, lesser amounts of massive gamma and supersaturated alpha-2 structures were observed compared to the microstructure obtained for 55 amps. A further increase in the welding current from 75 to 115 A produced a more extensive fusion zone with coarser grains.

## X-ray Diffraction Analysis of the Fusion Zone

XRD was utilized to determine the different phases that developed in the fusion zone microstructure. Figure 11 shows the results for spot welds obtained at three different heat inputs: 50, 100, and 150 A. The XRD data in this figure indicates there was a significant increase in the alpha-2 phase compared to the base metal condition — Fig. 2. This was revealed by the stronger peaks of the alpha-2 phase, especially the main peak in the (201) plane. The increase in alpha-2 structure was the highest for the 50-A specimen. This suggests the cooling rate plays an important role in the microstructural control of the fusion zone. In GTA welding of gamma Ti-

tanium aluminides, solid-state phase transformations are strongly affected by the cooling rates. At lower cooling rates, the lamellar structure is largely predominant. In this case, the alpha phase transforms into a well-defined alpha-2/gamma lamellar structure ( $\alpha \rightarrow \alpha + \gamma$ ). Studies have shown this reaction occurs in the two-phase  $\alpha + \gamma$  phase field of the TiAl phase diagram (Ref. 16) and exhibits characteristics of a nucleation and growth process, very likely involving diffusion (Ref. 17). At higher cooling rates, however, the decomposition of the alpha phase is suppressed in favor of the ordering of the alpha phase into the alpha-2 phase ( $\alpha \rightarrow \alpha_2$ ), resulting in an increased amount of alpha-two in the fusion zone. The present study suggests that welding of TiAl-based alloys should be conducted at cooling rates that will not suppress the decomposition of the alpha phase. In this work, the heat input or the applied welding current controlled the cooling rates. Moreover, the study of other variables that can also modify the cooling rates, such as welding speed and the use of preheating, was beyond the scope of this work.

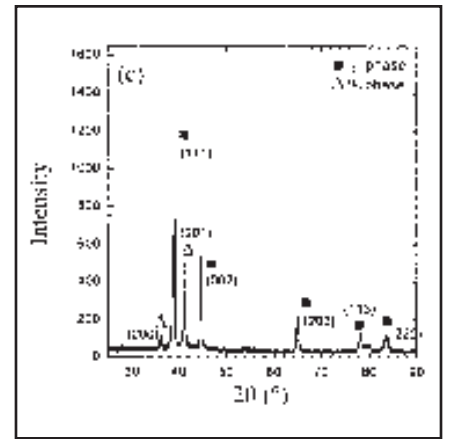
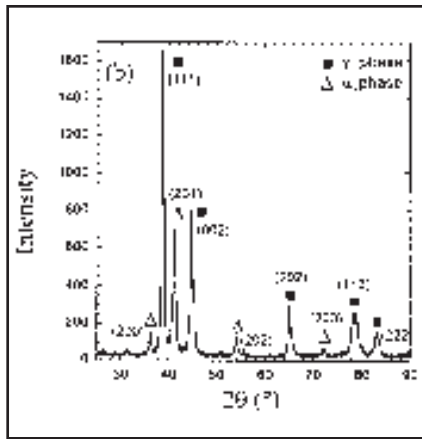
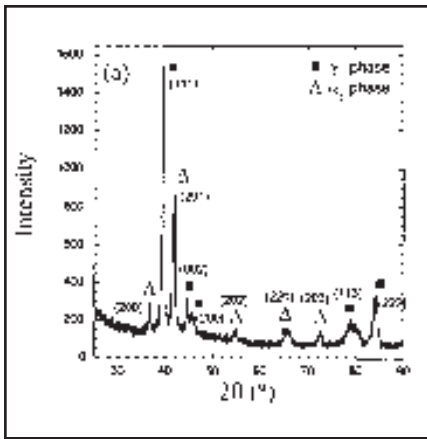


Fig. 11 — XRD patterns of the fusion zones obtained for different heat inputs. A — 50 A; B — 100 A; C — 150 A.

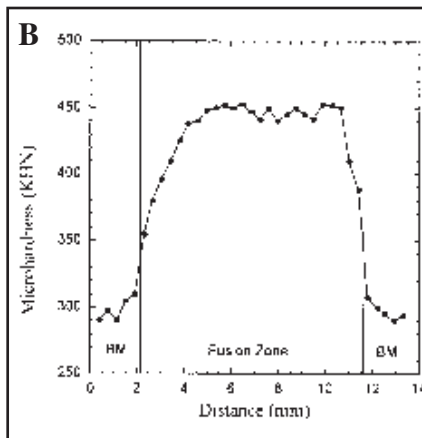
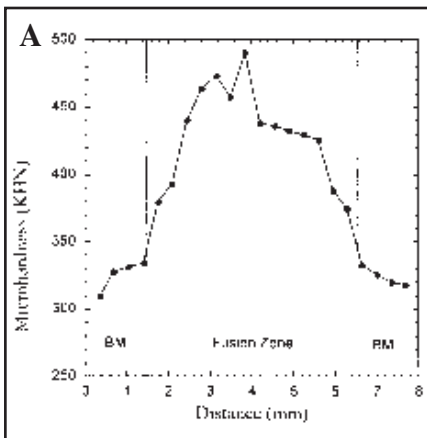


Fig. 12 — Microhardness profiles for welds produced at A — 75 A; B — 115 A.

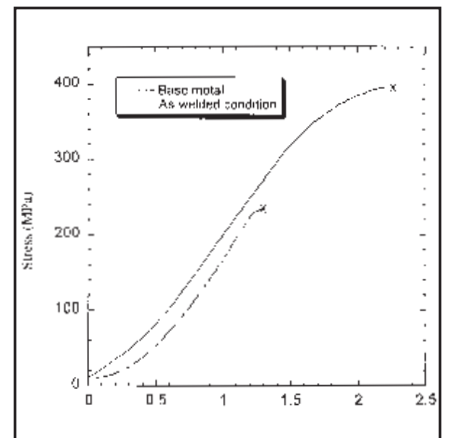


Fig. 13 — Stress-strain curves for the base metal and a specimen welded at 75 A.

## Microhardness Measurements

A microhardness profile of the as-welded condition using a heat input of 75 A is shown in Fig. 12A. In this figure, the fusion zone microhardness increased dramatically relative to the base metal microhardness of 300 KHN. The microhardness increased on average by a factor of 1.5. The observed increase in fusion zone microhardness is in agreement with all previous reports on TiAl weldability. It is believed the increase in microhardness is due to the increased presence of alpha-2 structures that formed during welding. This microstructure is known to have a higher microhardness compared to other gamma-related microstructures. The microhardness profile for the weld produced at 115 A is illustrated in Fig. 12B. This figure shows an increase in microhardness from the base metal to the fusion zone that was similar to the 75-A specimen. However, the average fusion zone microhardness was slightly lower than that observed

for the 75-A specimen, which corresponds with the decrease in alpha-2 phase that was observed as the welding current was increased — Fig. 11.

## Tensile Testing

Figure 13 shows the room temperature stress-strain curves for the as-welded condition and the as-received condition (base metal). Results show there was a dramatic decrease in tensile strength and loss of ductility for the as-welded condition. Furthermore, the calculated elongations at failure were 0.1 and 0.5% for the as-welded condition and the base metal, respectively. The observed tensile behavior of the as-welded condition agrees with the increase in fusion zone microhardness discussed previously.

The reduction of mechanical properties can be partially explained by the microstructural changes that occurred during welding that resulted in a higher amount of the brittle alpha-2 phase in the

fusion zone. SEM micrographs of the tensile test fracture surfaces for the as-received and as-welded specimens are shown in Fig. 14. For the welded specimen, fracture occurred in the weld fusion zone. The micrographs reveal that there are two distinct failure mechanisms for the base metal (Fig. 14A) and the as-welded condition (Fig. 14B). The base metal exhibited mainly translamellar fracture, which agrees with the great proportion of lamellar constituent in this material, as shown in Fig. 1. Translamellar fracture is associated with a greater degree of plastic deformation experienced at the crack tip and ligament formation, often yielding higher toughness. However, the as-welded condition exhibited transgranular cleavage fracture, which is common for brittle materials. The multifaceted surface, observed in Fig. 14B, is typical of cleavage in polycrystalline materials where each facet corresponds to a single grain. The “river patterns” on each face are also typical of cleavage fracture.

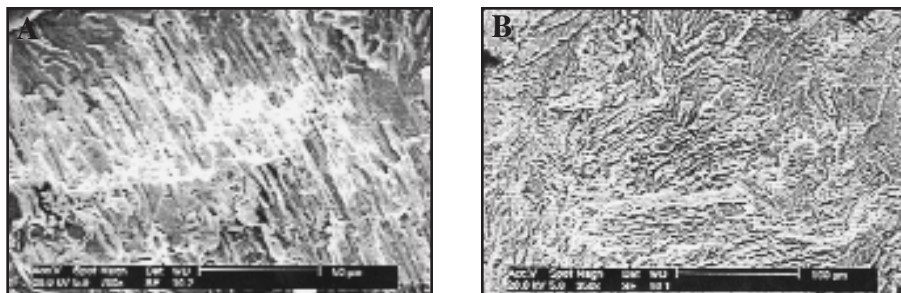


Fig. 14 — SEM secondary electron images of the tensile test fracture surfaces. A — As-received (base metal); B — as-welded conditions for TiAl. The as-received specimen shows translamellar fracture while the as-welded specimen exhibits transgranular cleavage-type fracture.

It is believed that fracture occurred in the planes with low cohesive strength. For TiAl, these planes have been identified as the  $(111)_\gamma$  planes (Ref. 18).

## Conclusions

Autogenous GTA welding has been used to produce crack-free welds in Ti-48Al-2Cr-2Nb without the use of preheating. A procedure for obtaining sound, crack-free welds consisted of pre-stress relief treatment of 615°C for 2 h and welding at arc currents equal to or greater than 75 A.

The  $\gamma$ -TiAl base metal microstructure consisted of a lamellar ( $\gamma/\alpha_2$ ) structure with some amount of gamma grains. However, the welded microstructure exhibited columnar and equiaxed dendritic structures. The columnar grains extended from the fusion boundary to the weld centerline, whereas the equiaxed structure developed at the center of the fusion zone. A closer examination of the dendritic grains showed they were composed of a considerably fine lamellar structure compared to that of the base metal. Other microstructural constituents observed in the fusion zone were supersaturated alpha-2 phases and massive gamma metastable structures. There were more of these structures present at the lower heat inputs. Less cracking was observed as the welding current was increased, which corresponded with a decrease in the alpha-2 phase in the fusion zone.

Mechanical properties of the weld were decreased relative to the base metal, as was indicated by microhardness measurements and tensile testing. A significant increase in microhardness was observed in the fusion zone. Also, the as-welded condition showed a reduction in ductility and a decrease in tensile strength.

### Acknowledgments

The authors gratefully acknowledge Tom J. Kelly and GE Aircraft Engines

(Cincinnati, Ohio) for donating the alloy used in this study. Financial support for this work was provided by the National Science Foundation under grant number DMR-9702448.

### References

- Kim, Y. -W., and Dimiduk, D. M. 1997. Designing gamma TiAl alloys: Fundamentals, strategy and production. *Structural Intermetallics 1997*, eds. M. V. Nathal, R. Darolia, C. T. Liu, P. L. Martin, D. B. Miracle, R. Wagner, and M. Yamaguchi. TMS, pp. 531-543.
- Kim, Y. -W. 1995. Trends in the development of gamma TiAl alloys. *Gamma Titanium Aluminides*, eds. Y. -W. Kim, R. Wagner, and M. Yamaguchi. TMS, pp. 637-654.
- Austin, C. M., and Kelly, T. J. 1995. Progress in implementation of cast gamma titanium aluminides. *Gamma Titanium Aluminides*, eds. Y. -W. Kim, R. Wagner, and M. Yamaguchi. TMS, pp. 21-32.
- Kim, Y. -W. 1999. Advances in the fundamental understanding for designing engineering gamma TiAl alloys. *Journal of Chinese Institute of Engineers* 22: 13-25.
- Tetsui, T. 1997. Application of cast gamma alloy for turbochargers. *Structural Intermetallics 1997*, eds. M. V. Nathal, R. Darolia, C. T. Liu, P. L. Martin, D. B. Miracle, R. Wagner, and M. Yamaguchi. TMS, pp. 489-493.
- Mallory, L., Baeslack III, W., and Phillips, D. 1994. Evolution of the weld heat-affected zone microstructure in a Ti-48Al-2Cr-2Nb gamma titanium aluminide. *Journal of Materials Science Letters* 13: 1061-1065.
- Mallory, L., Baeslack III, W., Phillips, D., and Kelly, T. 1993. Gas tungsten arc welding of a Ti-48Al-2Cr-2Nb gamma titanium aluminide. *Titanium 92, Science and Technology*, Vol. II, eds. F. Froes and I. Caplan. TMS, pp. 1115-1122.
- Kelly, T. 1992. Repair welding of gamma titanium aluminide castings. *Proc. 3rd International SAMPE Metals Conference*. SAMPE, pp. 183-191.
- Bharani, D. J., and Acoff, V. L. 1998. Autogenous gas tungsten arc weldability of cast alloy Ti-48Al-2Cr-2Nb (atomic percent) versus extruded alloy Ti-46Al-2Cr-2Nb-0.9Mo

(atomic percent). *Metallurgical Transactions A* 29A: 927-935.

10. Glatz, W., Retter, B., Leonhard, A., and Clemens, H. 1996. Problems relating to the metallographic preparation of  $\gamma$ -TiAl-base alloys. *Struers Journal of Metallography* 29: 3-7.

11. Austin, C. M., Kelly, T. J., McAllister, K. G., and Chesnutt, J. C. 1997. Aircraft engine applications for gamma titanium aluminide. *Structural Intermetallics 1997*, eds. M. V. Nathal, R. Darolia, C. T. Liu, P. L. Martin, D. B. Miracle, R. Wagner, and M. Yamaguchi. TMS, pp. 413-425.

12. Duwez, P., and Taylor, J. L. 1956. Crystal structure of TiAl. *Journal of Metals* 4: 70-71.

13. Goldak, A. J., and Parr, J. G. 1961. The structure of  $Ti_3Al$ . *AIME Transactions* 221: 639-640.

14. Patterson, R. A., Martin, P. L., Damkroger, B. K., and Christodoulou, L. 1990. Titanium aluminide: electron beam weldability. *Welding Journal* 69(1): 39-s to 44-s.

15. Lin, J. G., Wen, C. E., Zhang, Y. G., and Chen, C. Q. 1999. Diffusion ledge mechanism of massive  $\gamma$  transformation in quenched TiAl alloys. *Journal of Materials Science Letters*. 18(12): 927-929.

16. Palm, M., and Inden, G. 1997. Constitution of ternary aluminide systems as basis for materials development. *Structural Intermetallics 1997*, eds. M. V. Nathal, R. Darolia, C. T. Liu, P. L. Martin, D. B. Miracle, R. Wagner, and M. Yamaguchi. TMS, pp. 73-82.

17. Jones, S. A., and Kaufman, M. J. 1993. Phase equilibria and transformations in intermediate titanium-aluminum alloys. *Acta Metallurgica et Materialia* 41: 387-398.

18. Appel, F., and Wagner, R. 1998. Microstructure and deformation of two-phase  $\gamma$ -titanium aluminides. *Materials Science and Engineering R* 22 (5): 187-268.

## REPRINTS REPRINTS

To order custom reprints of  
articles in

*Welding Journal*

Contact Denis Mulligan at

(800) 259-0470

FAX: (717) 481-7677

or via e-mail at

info@reprintdept.com

## REPRINTS REPRINTS